Available online at www.sciencedirect.com

ScienceDirect

Ceramics International 40 (2014) 4567–4573

CERAMICS INTERNATIONAL

www.elsevier.com/locate/ceramint

Preparation, characterization and thermophysical properties of $(Sm_{1-x}Gd_x)_2Ce_2O_7$ solid solutions

Zhang Hongsong[a,*], Li Xiaochun[b], Li Gang[a], Li Zhenjun[a]

[a]Department of Mechanical Engineering, Henan Institute of Engineering, Zhengzhou 450007, China
[b]Department of Materials and Chemistry, Henan Institute of Engineering, Zhengzhou 450007, China

Received 7 August 2013; received in revised form 29 August 2013; accepted 29 August 2013
Available online 6 September 2013

Abstract

$Sm_2Ce_2O_7$ has low thermal conductivity and relatively high thermal expansion coefficient which make it suitable for application as high-temperature thermal barrier coatings. $(Sm_{1-x}Gd_x)_2Ce_2O_7$ solid solutions were synthesized by solid state reaction in this paper. The influence of Gd_2O_3-doping on the phase structure and thermophysical properties were investigated. The synthesized $(Sm_{1-x}Gd_x)_2Ce_2O_7$ ceramics exhibit a defect-fluorite structure, which is mainly determined by ionic radius ratio $r(A_{av}^{3+})/r(B^{4+})$. The linear thermal expansion coefficients and thermal conductivities of different $(Sm_{1-x}Gd_x)_2Ce_2O_7$ decrease with the increasing value of x in the measuring temperature. Their thermal expansion coefficients are higher than that of 8YSZ, the thermal conductivities of $(Sm_{1-x}Gd_x)_2Ce_2O_7$ ceramics at 1000 °C are located within the range of 1.07–1.69 W/m K. The composition dependence of thermal conductivity was discussed by taking into account the phonon scattering by mass and strain fluctuations at the A site.

Keywords: C. Thermal conductivity; C. Thermal expansion; Oxides; Thermal barrier coatings

1. Introduction

Thermal barrier coatings (TBCs) have been widely used to protect turbine engines operating in high temperature environment. Traditional TBCs consist of a ceramic top-coat (usually 100–400 μm thick) and an oxidation resistant bond-coat (~100 μm thick) which is usually deposited on nickel-based superalloy [1,2]. Due to low thermal conductivity, high phase stability, high thermal-expansion coefficient and high toughness compared to other ceramics, yttria-stabilized zirconia (YSZ) has been known as the most favorite top-layer material for many years [3,4]. The metallic coating acts not only as bond-coat but also as barrier against oxidation and corrosion of substrate at high temperature. The top-coat is mainly processed by air plasma spray (APS) and/or by electron beam physical vapor deposition (EB-PVD), while the bond-coat is deposited by various methods such as APS, high velocity oxy-fuel spray (HVOF), low pressure plasma spray (LPPS) and Pt-plating/chemical vapor deposition (CVD) or EB-PVD [5–7]. However, two flaws have been reported when YSZ are exposed to high temperature (above 1200 °C) for long time, i.e., phase transformation and sintering. Metastable tetragonal phase decomposes into tetragonal and cubic phase above 1200 °C. Upon cooling, tetragonal phase transforms to monoclinic phase, causing about 3.5% volume change and resulting in crack formation in the TBCs. In addition, volume fraction of pores decreases due to the significant sintering of YSZ at high temperature, which leads to an increase in the thermal conductivity as well as the in-plane stiffness and thus decreases the strain compliance of TBCs [5,6].

Due to the described shortcomings of YSZ, considerable efforts have been made to seek alternatives to further increase the gas turbine inlet temperature. However, the selection of TBCs materials is restricted by some basic requirements such as high melting point, low thermal conductivity, high thermal expansion coefficient, high phase stability, and low sintering rate [8–10]. It is found by many researchers that rare earth oxides with general composition of $A_2B_2O_7$ show promising thermophysical properties. In the type of $A_2B_2O_7$, A is a 3^+ cation (La–Lu) and B is a 4^+ cation (Zr, Hf, Sn, Ce, etc.) [11–13].

*Corresponding author. Tel.: +86 371 6250 8765.
E-mail address: zhs761128@163.com (Z. Hongsong).

0272-8842/$ - see front matter © 2013 Elsevier Ltd and Techna Group S.r.l. All rights reserved.
http://dx.doi.org/10.1016/j.ceramint.2013.08.133

The rare earth zirconates have excellent thermal stability, low sintering rate and low thermal conductivity. However, the low thermal expansion coefficient of rare earth zirconates leads to high thermal stress between the rare-earth zirconate coating and the metallic bond coat, resulting in a short thermal cycling life [8,10,12]. A few of rare-earth $A_2Hf_2O_7$ oxides have been proved to have lower thermal conductivity, better temperature phase stability compared to YSZ [14–17]. Unfortunately, most of current research results about thermophysical properties of rare-earth $A_2Hf_2O_7$ oxides are predicted by theoretical simulation calculation, there has been no further systemic experimental evidence to confirm the calculations [18,19]. Rare-earth stannates are a series of compounds with similar structures to the rare-earth zirconates. Interestingly, these compounds, $A_2Sn_2O_7$, constitute a complete series of isostructure compounds with a pyrochlore structure, whereas the rare-earth zirconates undergo a pyrochlore–fluorite transition, i.e. pyrochlores can only form for the lanthanide series from La to Gd, with the remainder existing as defective fluorites [20,21]. Thermophysical properties of some interesting rare-earth stannates, such as $La_2Sn_2O_7$, $Nd_2Sn_2O_7$, $Sm_2Sn_2O_7$, $Gd_2Sn_2O_7$, $Er_2Sn_2O_7$ and $Yb_2Sn_2O_7$, have been reported. However, their thermal conductivities are higher compared to 8YSZ (2.5–2.7 W/m K at 800 °C for $A_2Sn_2O_7$ and 2.1 W/m K at 1000 °C 8YSZ), and their thermal expansion coefficients are low compared to 8YSZ ($8.4–9.2 \times 10^{-6}\ K^{-1}$ at 1000 °C for $A_2Zr_2O_7$ and $10.1 \times 10^{-6}\ K^{-1}$ at 1000 °C for 8YSZ) [22]. These thermophysical properties imply that the stannates can not be explored as candidate materials for the ceramic layer in TBC system.

In recent years, rare-earth $A_2Ce_2O_7$ oxides have attracted extensive attention due to their excellent electrical, catalytic, mechanical properties, low thermal conductivities and high thermal expansion coefficients at high temperature. Thermophysical properties of several interesting rare earth cerium oxides, such as $La_2Ce_2O_7$ [23,24], $Nd_2Ce_2O_7$ [25], $Gd_2Ce_2O_7$ [26,27], $Y_2Ce_2O_7$ [28], $Dy_2Ce_2O_7$ [29], $Sm_2Ce_2O_7$, $Er_2Ce_2O_7$ and $Yb_2Ce_2O_7$ [30] have been investigated. Results indicate that these rare earth cerium oxides have potential to be used as new candidate materials for future TBCs. It is well known that materials with lower thermal conductivity and higher thermal expansion coefficient can be prepared by doping or co-doping with one more oxides (Yb_2O_3, Gd_2O_3, Sm_2O_3 and Nd_2O_3) due to defect cluster formation, which indicates that the thermal conductivity of $A_2Ce_2O_7$ oxides can be reduced further by doping with other elements in the cation of A or Ce [31,32]. Clarke and coworkers also point out that substituted cations, especially the atom with large atomic weight, at site A or B creates mass disorder on the cation sublattice, which results in the lowering of thermal conductivity [31]. Meanwhile the thermal expansion coefficient is proved to be higher by Cao et al. [25]. According to this theroy, thermophysical properties of Gd-doped $La_2Ce_2O_7$ have been reported in Ref. [24], the evident differences in ionic radius and mass weight lead to the decreasing thermal conductivity of $(La_{1-x}Gd_x)_2Ce_2O_7$, and their thermal expansion coefficients are still higher than that of 8YSZ. In the lanthanide elements, ionic radius and mass weight of samarium and gadolinium are very close, $(Sm_{1-x}Gd_x)_2Zr_2O_7$ ($x=0$, 0.2, 0.4, 0.6, 0.8 and 1) and $(Sm_xGd_{1-x})_2Zr_2O_7$ ceramics have been synthesized and their thermophysical properties were studied, the relatively mass differences (mass fluctuation), and size and interatomic coupling force differences (strain filed fluctuations) contribute the decreasing thermal conductivities of $(Sm_{1-x}Gd_x)_2Zr_2O_7$ and $(Sm_xGd_{1-x})_2Zr_2O_7$ ceramics [33]. The $(Sm_{1-x}Gd_x)_2Zr_2O_7$ or $(Sm_xGd_{1-x})_2Zr_2O_7$ ceramics are rare earth zirconates, however, the influence of $(Sm_{1-x}Gd_x)_2Ce_2O_7$ ceramics have not been reported in open literatures.

In this paper, $(Sm_{1-x}Gd_x)_2Ce_2O_7$ ceramics were prepared by the solid reaction method. The structure evolution and thermophysical properties of $(Sm_{1-x}Gd_x)_2Ce_2O_7$ ceramics were investigated in order to understand on co-doped fluorite-structure rare-earth cerium oxides.

2. Experimental

In the present study, CeO_2, Gd_2O_3 and Sm_2O_3 (Rare-Chem Hi-Tech Co., Ltd., Huizhou, China; purityHi-Tec) were chosen as the reactants. The oxides powders were fired at 1000 °C for 5 h before weighting in order to eliminate hydroxide and/or carbonate. After mixed the stoichiometric constituents of $(Sm_{1-x}Gd_x)_2Ce_2O_7$ by ball milling in analytically pure alcohol and dried at 110 °C for 5 h. The dried powder mixtures were then sieved for granulation and compressed into a disk form under uniaxial pressure of 50 MPa by cold isostatic pressing with 150 MPa. The bulks were placed on cerium tiles and sintered at 1600 °C for 10 h in air. The pellets were subsequently cooled in air at the end.

For heat-treated samples, the actual densities were measured by the Archimedes method with an immersion medium of deionized water. The phases of heat-treated samples were identified using an X-ray diffraction (XRD, X'Pert PRD MPD The Netherlands) with Ni filtered CuKα radiation (0.1542 nm) at the scanning rate of 4°/min. The lattice parameters of developed phases were calculated from the XRD results. The theoretical density of each composition was calculated using lattice parameters acquired from XRD results and the molecular weight in an elementary cell. Scanning electron microscopy (SEM, Model Hitachi S-4800, Japan) was used to observe the microstructure of bulk ceramics. The specimens were polished with 1 μm diamond paste, and then thermally etched at 1500 °C for 2 h in air for SEM observations. Qualitative element analysis of various phases was carried out using SEM equipped with energy dispersive spectroscopy (EDS).

The thermal diffusivity (λ) of the synthesized samples was measured using laser-flash method (Model Netzsch LFA 427/) in the range 200–1000 °C in an argon atmosphere 7/G. The sample dimension for thermal diffusivity measurement was about 12.7 mm in diameter and about 1 mm in thickness. Before thermal diffusivity measurement, both the front and back faces of the samples were coated with a thin layer of graphite. These coatings were done to prevent direct transmission of laser beam through the translucent specimens. The specific heat capacity (C_p) as a function of temperature was calculated from the heat

capacity data of the constituent oxides of $(Sm_{1-x}Gd_x)_2Ce_2O_7$, in conjunction with the Neumann–Kopp rule [34] and the heat capacity data of the constituent oxides (Sm_2O_3, Gd_2O_3 and CeO_2) were obtained from the literature [35]. The thermal conductivity (k) of the specimen was calculated by Eq. (1) with specific heat capacity (C_p), density (ρ) and thermal diffusivity (λ).

$$k = \lambda \rho C_P \quad (1)$$

Because the sintered specimen was not full dense, the measured thermal conductivity were modified for the actual value k_0 using Eq. (2), where ϕ is the fractional porosity and the coefficient 4/3 is used to eliminate the effect of porosity on actual thermal conductivity [23].

$$\frac{k}{k_0} = 1 - \frac{4}{3}\phi \quad (2)$$

The linear thermal expansion coefficient (TEC) of the sintered samples was determined with a high-temperature dilatometer (Model NeTZSCH DIL 402C/7, Germany). The size of sample was approximately $25 \times 3 \times 4 mm^3$. Data for precise calculation of thermal expansion coefficient were measured in the temperature range of ambient and 1000 °C at a heating rate of 5 °C/min in argon atmosphere, and they were corrected using the known thermal expansion of a certified standard alumina.

3. Results and discussion

3.1. XRD

Fig. 1 reveals the room temperature X-ray diffraction patterns of $(Sm_{1-x}Gd_x)_2Ce_2O_7$ $(0 \le x \le 0.5)$ ceramics sintered at 1600 °C for 10 h in air. It can be seen that $(Sm_{1-x}Gd_x)_2Ce_2O_7$ $(0 \le x \le 0.5)$ ceramics have a single phase structure, and there are no any additional weak peaks in the 2θ range of 40°–50° in their XRD patterns, which can help us to distinguish the fluorite and the pyrochlore structures.

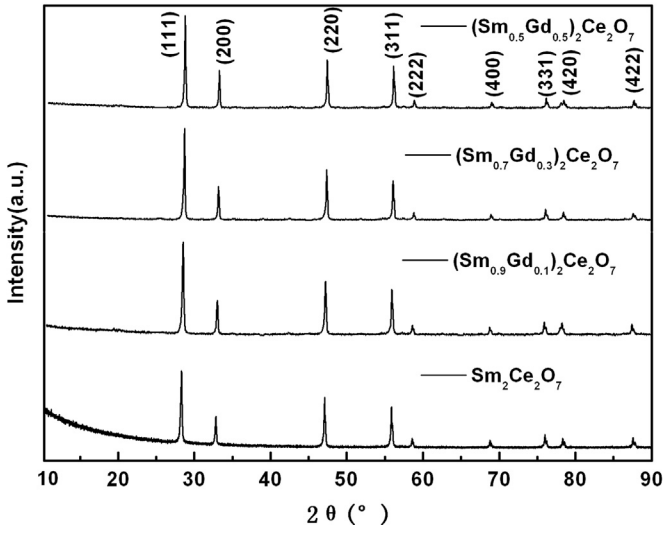

Fig. 1. XRD patters of $(Sm_{1-x}Gd_x)_2Ce_2O_7$ bulk ceramics.

In rear earth $A_2B_2O_7$ (A = rear earth element, B = Zr, Ce, Hf and Sn)-type oxides, the phase structure is mainly governed by the ionic radius ratio of $r(A^{3+})/r(B^{4+})$. The stability of pyrochlore-type structure is limited to the range of $1.46 \le r(A^{3+})/r(B^{4+}) \le 1.78$ at an atmospheric pressure. Below 1.46, the array of unoccupied anion sites disorders, to produce a defect fluorite structure. Above 1.78, there is a transition to a monoclinic phase structure [36]. The ionic radius of Ce^{4+} is 0.097 nm, however, the ionic radii of Sm^{3+} and Gd^{3+} are 0.1079 and 0.1053 nm, respectively [37]. The average ionic radius, $r(A_{av}^{3+})$, of the A-sites in the $(Sm_{1-x}Gd_x)_2Ce_2O_7$ $(0 \le x \le 0.5)$ ceramics is estimated from the ionic radii of the component ions and the chemical composition using the following equation [24]:

$$r(A_{av}) = xr(Gd^{3+}) + (1-x)r(Sm^{3+}) \quad (3)$$

The ratio values of $r(A^{3+})/r(B^{4+})$ are clearly lower than 1.46 for $(Sm_{1-x}Gd_x)_2Ce_2O_7$ $(0 \le x \le 0.5)$ ceramics, respectively, and therefore $(Sm_{1-x}Gd_x)_2Ce_2O_7$ $(0 \le x \le 0.5)$ ceramics exhibit a defect fluorite-type structure. The lattice parameters of $(Sm_{1-x}Gd_x)_2Ce_2O_7$ $(0 \le x \le 0.5)$ ceramics calculated from their X-ray diffraction peaks in relation to the fluorite-type unit cell are 0.549, 0.5488, 0.548 and 0.5475 nm. An approximately linear decrease of the lattice parameters is observed for $(Sm_{1-x}Gd_x)_2Ce_2O_7$ $(0 \le x \le 0.5)$ ceramics with increasing gadolinium content, which is in a good agreement with the Vegard's rule.

3.2. SEM

Fig. 2 presents the typical micro-morphologies of $(Sm_{1-x}Gd_x)_2Ce_2O_7$ $(0 \le x \le 0.5)$ ceramics sintered at 1600 °C for 10 h. As can be seen from Fig. 2, the grain size and morphology of $(Sm_{1-x}Gd_x)_2Ce_2O_7$ $(0 \le x \le 0.5)$ ceramics with different compositions are very similar. The average size of $(Sm_{1-x}Gd_x)_2Ce_2O_7$ ceramics is several micro-meters, and the grain boundaries of $(Sm_{1-x}Gd_x)_2Ce_2O_7$ ceramics are very clean, no other inter-phases or unreacted oxides exist in the interfaces. With increasing gadolinium content, the absolute densities of $(Sm_{1-x}Gd_x)_2Ce_2O_7$ solid solutions are 6.69, 6.75, 6.79 and 6.91 g/cm^3. Their relative densities measured by using the Archimedes method in sequence are 96.2%, 96.75%, 96.5% and 97.5%, which shows that $(Sm_{1-x}Gd_x)_2Ce_2O_7$ $(0 \le x \le 0.5)$ ceramics have a dense microstructure. The chemical compositions of the synthesized oxides were determined using EDS and Table 1 shows the results of chemical compositions for $(Sm_{1-x}Gd_x)_2Ce_2O_7$ ceramics. According to EDS analysis, the mole ratio of different elements in $(Sm_{1-x}Gd_x)_2Ce_2O_7$ ceramics is very close to their stoichiometery.

3.3. Thermal expansion coefficient

The thermal expansion coefficient is also of great importance for thermal barrier coating materials, since they are in contact with a metallic substrate, and a high thermal expansion coefficient is required to minimize the thermal mismatch between the ceramic coating and the substrate [38]. The results of the dilatometric measurement for $(Sm_{1-x}Gd_x)_2Ce_2O_7$ $(0 \le x \le 0.5)$ solid solutions

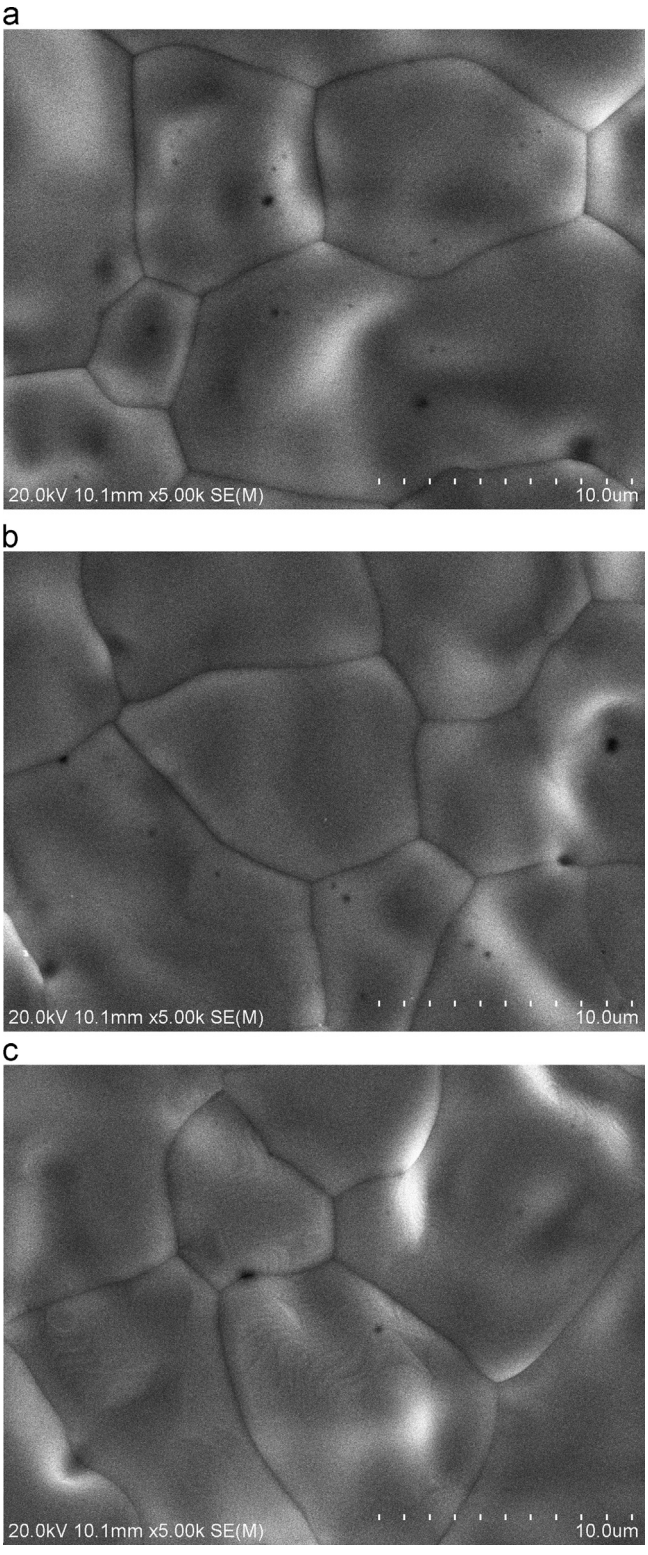

Fig. 2. Microstructure of synthesized oxides, (a) $(Sm_{0.9}Gd_{0.1})_2Ce_2O_7$, (b) $(Sm_{0.7}Gd_{0.3})_2Ce_2O_7$ and (c) $(Sm_{0.5}Gd_{0.5})_2Ce_2O_5$.

with calibration are shown in Fig. 3. The typical linear expansion are observed for $(Sm_{1-x}Gd_x)_2Ce_2O_7$ $(0 \le x \le 0.5)$ solid solutions in the temperature range of ambient − 1000 °C. Clearly, there is no phase transformation for $(Sm_{1-x}Gd_x)_2Ce_2O_7$ $(0 \le x \le 0.5)$ ceramics from ambient to 1000 °C. The technical thermal expansion

Table 1
Atomic percentages of bulk samples of $(Sm_{1-x}Gd_x)_2Ce_xO_7$ solid solutions.

Ceramic bulk materials	Element mole ratio			
	Sm	Gd	Ce	O
$Sm_2Ce_2O_7$	17.8	0	17.6	64.6
$(Sm_{0.9}Gd_{0.1})_2Ce_2O_7$	13.4	2.2	18.5	65.9
$(Sm_{0.7}Gd_{0.3})_2Ce_2O_7$	10.4	5.1	19.1	65.4
$(Sm_{0.5}Gd_{0.5})_2Ce_2O_7$	6.9	8.7	18.9	65.5

coefficient is defined as:

$$\alpha_{tech} = \frac{1}{L_0}\frac{\Delta L_k - \Delta L_0}{T_k - T_0} \quad (4)$$

where L_0 is the length of the specimen at T_0(20 °C), ΔL_0 is the change in length at T_0, and ΔL_k is the corresponding length change at temperature T_k.

The calculated technical thermal expansion coefficients of $(Sm_{1-x}Gd_x)_2Ce_2O_7$ $(0 \le x \le 0.5)$ ceramics as a function of temperature are presented in Fig. 4. The technical thermal expansion coefficients of $(Sm_{1-x}Gd_x)_2Ce_2O_7$ $(0 \le x \le 0.5)$ ceramics increase gradually with the increase of temperature, which is attributed to the increasing atomic spacing at elevated temperatures. The technical thermal expansion coefficients of $(Sm_{1-x}Gd_x)_2Ce_2O_7$ $(0 \le x \le 0.5)$ ceramics rapidly increase from 50 °C to about 300 °C, which is caused by nonlinear increase of the instrument temperature, and similar phenomenon was also reported by Qin et al. [39,40]. Above 300 °C, the technical thermal expansion coefficients of $(Sm_{1-x}Gd_x)_2Ce_2O_7$ $(0 \le x \le 0.5)$ ceramics gradually decrease with increasing gadolinium content at identical temperature levels. This phenomena can be attributed the lower ionic radius of Gd^{3+} (1.053 Å) than that of Sm^{3+} (1.079 Å). There are some structure defects, such as substitutional or interstitial cations and other imperfections in the lattice or varying properties in thermal expansion along with different orientations that have significant effect on the overall thermal expansion coefficient of $A_2B_2O_7$ oxides [41]. In the $Ln_2Ce_2O_7$ system, oxygen vacancies are randomly distributed in disordered fluorite structure, therefore it facilitates formation of the ionic vacancy clustering, which represents to some extent the decrease in thermal expansion. The higher the Gd content in $(Sm_{1-x}Gd_x)_2Ce_2O_7$ is, the higher the structure disorder degree is, and the more ionic vacancy clustering is created. In addition, the substitution of Sm^{3+} by Gd^{3+} can lead to the crystal lattice vibration reduced, hence $(Sm_{1-x}Gd_x)_2Ce_2O_7$ ceramics have decreasing thermal expansion coefficients with increasing Gd_2O_3 content.

The technical thermal expansion coefficients of $(Sm_{1-x}Gd_x)_2Ce_2O_7$ $(0 \le x \le 0.5)$ ceramics at 1000 °C are 11.84×10^{-6}, 11.8×10^{-6}, 11.71×10^{-6} and 11.52×10^{-6}/K. These thermal expansion coefficients are obviously higher than 7 wt% yttria stabilized zirconia (10.7×10^{-6}/K at 1000 °C [10]) and are good enough to be used as thermal barrier coatings materials in the industry condition.

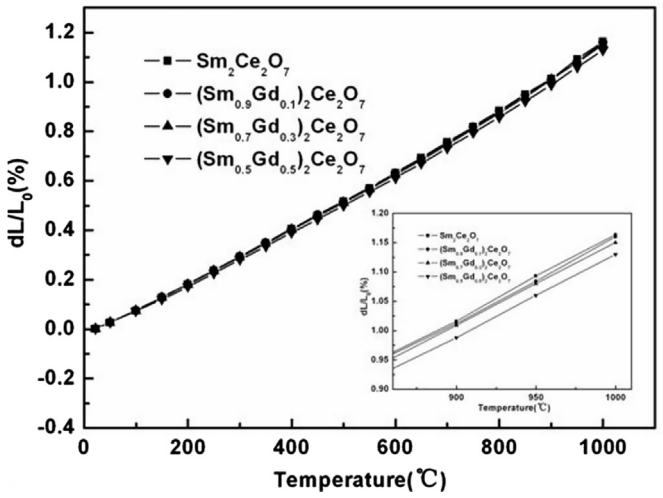

Fig. 3. Calibrated dilatometric data of $(Sm_{1-x}Gd_x)_2Ce_2O_7$ ceramics as a function of temperature.

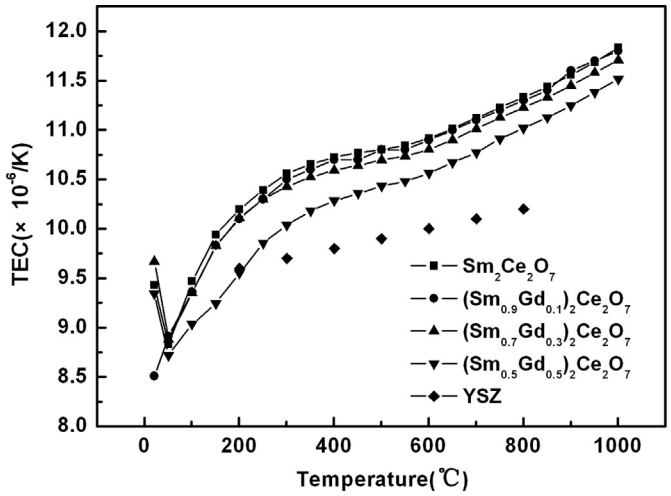

Fig. 4. Technical thermal expansion coefficient of $(Sm_{1-x}Gd_x)_2Ce_2O_7$ as a function of temperature.

3.4. Thermal conductivity

The calculated specific heat capacities of $(Sm_{1-x}Gd_x)_2Ce_2O_7$ based on Neumann–Kopp rule at different temperatures were shown in Table 2. The thermal diffusivities of different $(Sm_{1-x}Gd_x)_2Ce_2O_7$ bulk ceramics as a function of temperature are shown in Fig. 5. The values for thermal diffusivities exhibiting in Fig. 5 are the arithmetic means of the three measurements. The error bars are omitted as they are smaller than the symbols. It can be seen that the thermal diffusivities decrease with increase of temperature from 200 °C to 1000 °C, which suggests a dominant phonon conduction behavior in the most polycrystalline materials [42]. In this investigation, the measured thermal diffusivities of $(Sm_{1-x}Gd_x)_2Ce_2O_7$ are located within the range of 0.457–1.1 $mm^2 s^{-1}$ from 200 °C to 1000 °C, and the $(Sm_{0.5}Gd_{0.5})_2Ce_2O_7$ shows the lowest thermal diffusivity among these ceramics.

The thermal conductivities of $(Sm_{1-x}Gd_x)_2Ce_2O_7$ ceramics as a function of temperature are plotted in Fig. 6 according to

Table 2
Specific heat capacities of $(Sm_{1-x}Gd_x)_2Ce_xO_7$ solid solutions calculated with Neumann–Kopp rule at different temperatures.

Ceramic bulk materials	Specific heat capacities ($J\,g^{-1}\,K^{-1}$)				
	200 °C	400 °C	600 °C	800 °C	1000 °C
$Sm_2Ce_2O_7$	0.389	0.411	0.431	0.451	0.471
$(Sm_{0.9}Gd_{0.1})_2Ce_2O_7$	0.389	0.409	0.430	0.450	0.470
$(Sm_{0.7}Gd_{0.3})_2Ce_2O_7$	0.387	0.408	0.428	0.449	0.469
$(Sm_{0.5}Gd_{0.5})_2Ce_2O_7$	0.386	0.407	0.427	0.447	0.467

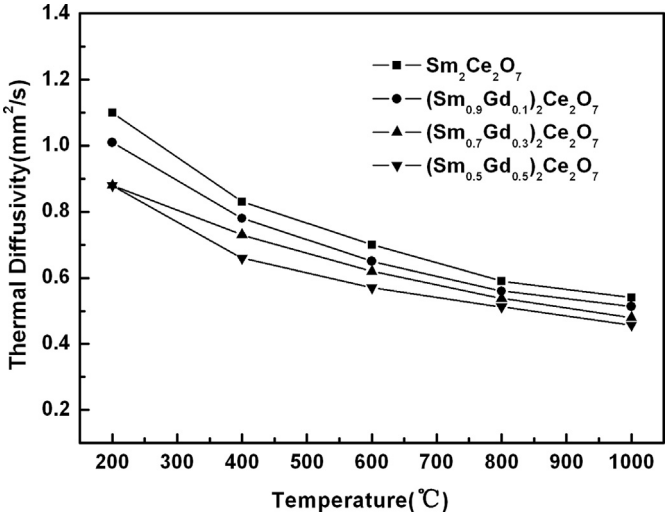

Fig. 5. Thermal diffusivities of $(Sm_{1-x}Gd_x)_2Ce_2O_7$ ceramics for different temperatures.

Eq. (1) with the specific heat capacity (C_p), density (ρ) and thermal diffusivity (λ). The values Fig. 6 were corrected to 100% theory density according to Eq. (2). It can be noted that the thermal conductivities of these ceramics decrease gradually as temperature increases almost throughout the present temperature range. From Fig. 6, doping of Gd_2O_3 clearly reduces thermal conductivities of $(Sm_{1-x}Gd_x)_2Ce_2O_7$ solid solutions and $SmGdCe_2O_7$ ceramic has the lowest thermal conductivity in this investigation. According to the micro-mechanism of thermal conduction, the thermal conduction of inorganic nonmetallic material is the result of phonon impacting, and the thermal conductivity (k) of phonon is shown by the following equation [30]:

$$k = \frac{1}{3} C_v v \bar{l} \tag{5}$$

where C_v is the specific heat capacity of the phonon, v is the velocity of phonon, and $\bar{l}$ is the mean free path of phonon. Above Dybye temperature, C_v is almost a constant. The value of v is related with elastic ratio (E) and density (ρ), because of the influence of temperature on the elastic ratio and density is not obvious, so the value of v may be also as a constant approximately. Consequently, the value of thermal conductivity (k) is mainly decided by the phonon mean free path. In real crystal structures, lattice imperfections, such as point defect

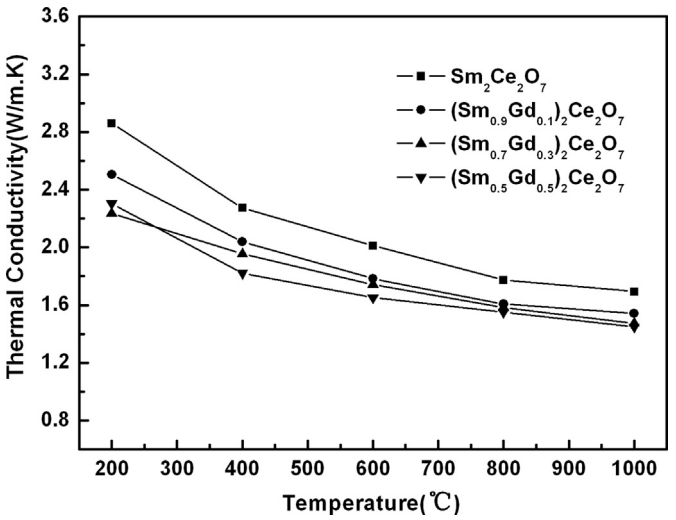

Fig. 6. Temperature dependence of thermal conductivity of $(Sm_{1-x}Gd_x)_2Ce_2O_7$ ceramics.

and grain boundary, can reduce the phonon mean free path by effective phonon scattering. As seen in Fig. 3, the current samples have grain size in the micrometer range. The decrease of the thermal conductivity due to the phonon scattering at grain boundary is not expected in the case of the ceramic materials investigated here. The lattice imperfections in the solid solution are caused by substitution of Sm^{3+} by Gd^{3+} in $Sm_2Ce_2O_7$. Thermal conduction owing to the changes of lattice virbrations may be affected by point defect scattering for phonons including mass differences (mass fluctuations), and size and interatomic coupling force differences (strain filed fluctuations) which can decrease the mean free path [41]. Thus, thermal conductivity was highest in pure compounds, and decreased as Gd_2O_3 were introduced into the crystals. The thermal conductivities of $(Sm_{1-x}Gd_x)_2Ce_2O_7$ ceramics in this investigation were located within the range of 1.44–2.85 W/m K from 200 to1000 °C, which are clearly lower than that of full dense 7 wt%Y_2O_3–ZrO_2 (3.0 at room temperature to 2.3 W/m K at 700 °C reported by Wu et al. [12]). Thus, $(Sm_{1-x}Gd_x)_2Ce_2O_7$ ceramics are potential candidates for high-temperature thermal insulation applications.

4. Conclusions

$(Sm_{1-x}Gd_x)_2Ce_2O_7$ solid solutions have been successfully synthesized. The solid solutions $(Sm_{1-x}Gd_x)_2Ce_2O_7$ have a defect-fluorite structure. Their thermal expansion coefficients decrease with increasing Gd_2O_3 content because of the lower ionic radius of Gd^{3+} as compared to Sm^{3+}. The decreasing thermal conductivity of the solid solutions is mainly related the point defect phonon scattering. However, their thermal expansion coefficients are higher than that of 8YSZ, and their thermal conductivities are lower than that of 8YSZ. Their excellent thermophysical properties indicate that the solid solutions $(Sm_{1-x}Gd_x)_2Ce_2O_7$ show promise as TBC materials.

Acknowledgments

The authors gratefully acknowledge financial sponsored by Program for Science & Technology Innovation Talents in Universities of Henan Province (13HASTIT018) and Key Project in Science and Technology of Henan Province (132102210142)

References

[1] C. Zhu, P. Li, A. Jived, G.Y. Liang, P. Xiao, An investigation on the microstructure and oxidation behavior of laser remelted air plasma sprayed thermal barrier coatings, Surface and Coatings Technology 206 (2012) 3739–3746.
[2] B.R. Marple, R.S. Lima, C. Moreau, S.E. Kruger, L. Xie, M.R. Dorrman, Yttria-stabilized zirconia thermal barrier sprayed using N_2–H_2 and Ar–H_2 plasmas: Influence of processing and heat treatment on coating properties, Journal of Thermal Spray Technology 16 (2007) 791–797.
[3] W.G. Mao, J.P. Jiang, Y.C. Zhou, C. Lu, Effects of substrate curvature radius, deposition temperature and coating thickness on the residual stress field of cylindrical thermal barrier coatings, Surface and Coatings Technology 205 (2011) 3093–3102.
[4] J.M. Drexler, K. Shinoda, A.L. Ortiz, D.S. Li, A.L. Vasiliev, A. D. Gledhill, S. Sampath, N.P. Padiure, Air-plasma-sprayed thermal barrier coatings that are resistant to high-temperature attack by glass deposits, Acta Materialia 58 (2010) 6835–6844.
[5] L. Liu, H.F. Zhang, X.G. Lei, Y.F. Zheng, Dependence of microstructure and thermal conductivity of EB-PVD thermal barrier coatings on the substrate rotation speed, Physics Procedia 18 (2011) 206–210.
[6] W. Chi, S. Sampath, H. Wang, Ambient and high-temperature thermal conductivities of thermal sprayed coatings, Journal of Thermal Spray Technology 15 (2006) 773–778.
[7] L.J. Gu, X.L. Chen, X.Z. Fan, Y.J. Liu, B.L. Zou, Y. Wang, X.Q. Cao, Improvement of thermal shock resistance for thermal barrier coating on aluminum alloy with various electroless interlayers, Surface and Coatings Technology 206 (2011) 29–36.
[8] J.Y. Xiang, S.H. Chen, J.H. Huang, H. Zhang, X.K. Zhao, Phase structure and thermophysical properties of co-doped $La_2Zr_2O_7$ ceramics for thermal barrier coatings, Ceramics International 38 (2012) 3607–3612.
[9] V.K. Tolpygo, D.R. Clarke, Morphological evolution of thermal barrier coatings induced by cyclic oxidation, Surface and Coatings Technology 163-164 (2003) 81–86.
[10] X.Q. Cao, R. Vassen, D. Stoever, Ceramic materials for thermal barrier coatings, Journal of the European Ceramic Society 24 (2004) 1–10.
[11] C.R. Stanek, L. Minervini, R.W. Grimes, Nonstoichimetry in $A_2B_2O_7$ pyrochlores, Journal of the American Ceramic Society 85 (2002) 2792–2798.
[12] J. Wu, X.Z. Wei, N.P. Padture, P.G. Klemens, M. Gel, E. Garcia, P. Miranzo, M.I. Osendi, Low thermal conductivity rare-earth zirconates for potential thermal barrier coating applications, Journal of the American Ceramic Society 85 (2002) 3031–3035.
[13] F.W.B. Lopes, C.P.D. Souza, A.M.V.D. Morais, J.P. Dallas, J.R. Gavarri, Determination of $RE_2Ce_2O_7$ pyrochlores phases from monazite–allanite ores, Hydrometallurgy 97 (2009) 167-172 97.
[14] K.R. Whittle, L.M.D. Cranswick, S.A.T. Redfern, L.P. Swainson, Lanthanum pyrochlores and the effect of yttrium addition in the systems $La_{2-x}Y_xZr_2O_7$ and $La_{2-x}YHf_2O_7$, Journal of Solid State Chemistry 182 (2009) 442–450.
[15] C.K. Roy, M.N.A. Alam, A.R. Choudhuri, C.V. Ramana, Synthesis and microstructure of Gd_2O_3-doped HfO_2 ceramics, Ceramics International 38 (2012) 1801–1806.
[16] H. Ibegazene, S. Alperine, C. Diot, Yttria-stabilized hafnia-zirconia thermal barrier coatings: the influence of hafnia addition on TBC structure and high temperature behavior, Journal of Materials Science 30 (1995) 938–951.
[17] J. Singh, D.E. Wolfe, R.A. Miller, Tailored microstructure of zirconia and hafnia-based thermal barrier coatings with low thermal conductivity and

high hemispherical reflectance by EB-PVD, Journal of Materials Science 39 (2004) 1975–1985.
[18] B. Liu, J.Y. Wang, F.Z. Li, Y.C. Zhou, Theoretical elastic stiffness, structural stability and thermal conductivity of $La_2T_2O_7$ (T=Ge, Ti, Sn, Zr and Hf) pyrochlore, Acta Materialia 58 (2010) 4369–4377.
[19] C.R. Stanek, R.W. Grimes, Prediction of rare-earth $A_2Hf_2O_7$ pyrochlore phases, Journal of the American Ceramic Society 85 (2002) 2139–2141.
[20] K.W. Li, H. Wang, H. Yan, Hydrothermal preparation and photocatalytic properties of $Y_2Sn_2O_7$ nanocrystals, Journal of Molecular Catalysis A: Chemical 249 (2006) 65–70.
[21] K.W. Li, H. Wang, H. Yan, Low temperature synthesis and structure characterization of the series $Y_2Bi_\delta Sn_2O_7$ (δ=0–2.0) nanocrystal, Journal of Solid State Chemistry 179 (2006) 1029–1034.
[22] Z.X. Qu, C.L. Wan, W. Pan, Thermophysical properties of rare-earth stagnates: effect of pyrochlore structure, Acta Materialia 60 (2012) 2939–2949.
[23] Z.H. Song, W. Yuan, L. Gang, C.X. Ge, W.X. Li, Investigation about thermal conductivities of $La_2Ce_2O_7$ doped with calcium or magnesium for thermal barrier coatings, Journal of Alloys and Compounds 537 (2012) 141–146.
[24] Z.H. Song, C.X. Ge, L. Gang, W.X. Li, D.X. Dan, Influence of Gd_2O_3 addition on thermophysical properties of $La_2Ce_2O_7$ ceramics for thermal barrier coatings, Journal of the European Ceramic Society 32 (2012) 3693–3700.
[25] H. Dai, X.H. Zhong, J.Y. Li, J. Meng, X.Q. Cao, Neodymium–cerium oxides as new thermal barrier coatings material, Surface and Coatings Technology 201 (2006) 2527–2533.
[26] S.J. Patwe, B.R. Ambekar, A.K. Tyagi, Synthesis, characterization and lattice thermal expansion of some compounds in the system $Gd_2Ce_xZr_{2-x}O_7$, Journal of Alloys and Compounds 389 (2005) 243–246.
[27] H.S. Zhang, S.R. Liao, X.D. Dang, S. Kang., Z. Guan, Zhang, Preparation and thermal conductivities of $Gd_2Ce_2O_7$ and $(Gd_{0.9}Ca_{0.1})_2Ce_2O_{6.9}$ ceramics for thermal barrier coatings, Journal of Alloys and Compounds 509 (2011) 1226–1230.
[28] H.S. Zhang, S.R. Liao, W. Yuan, S.K. Guan, Preparation and thermal conductivity of $Y_2Ce_2O_7$ ceramic material, Advanced Materials Research 266 (2011) 59–62.
[29] Z.H. Song, L.S. Ran, G.S. Kang, Preparation and thermal conductivity of $Dy_2Ce_2O_7$ ceramic material, Journal of Materials Engineering and Performance 21 (2012) 1046–1050.
[30] Z.H. Song, L.J. Guo, L. Gang, Z. Zheng, W.X. Li, Investigation about thermophysical properties of $Ln_2Ce_2O_7$ (Ln=Sm, Er and Yb) oxides for thermal barrier coatings, Materials Research Bulletin 47 (2012) 4181–4186.
[31] M.R. Winter, D.R. Clarke, Oxides materials with low thermal conductivity, Journal of the American Ceramic Society 90 (2007) 533–540.
[32] H.S. Zhang, S.R. Liao, Y. Wei, S.K. Guan, Methods to reduce thermal conductivity further of plasma sprayed thermal barrier coatings, Advanced Materials Research 230–232 (2011) 49–53.
[33] Z.G. Liu, J.H. Ooyang, Y. Zhou, Structural evolution and thermophysical properties of $(Sm_xGd_{1-x})_2Zr_2O_7$ (0uc $\leq$ 1.0) ceramics, Journal of Alloys and Compounds 472 (2009) 319–325.
[34] J.D. Leitner, P. Chuchvalec, D. Sedmidubsky, Estimation of heat capacity of solid mixed oxides, Thermochimica Acta 395 (2003) 27–46.
[35] O. Kubaschewsji, C.B. Alcock, P.J. Spencer, Materials Thermochemistry, sixth Ed., Pergamon Press, Oxford, 1993.
[36] M.A. Subramanian, G.S. Aravamudan, G.V. Subbarao, Oxides pyrochlore—a review, Progress in Solid State Chemistry 15 (1983) 55–143.
[37] Z.G. Liu, J.H. Ouyang, K.N. Sun, X.L. Xia, Effect of Gd and Yb co-doping on structure and electrical conductivity of $Sm_2Zr_2O_7$ pyrochlore, Journal of Power Source 195 (2010) 7225–7229.
[38] N.P. Padture, M. Gell, E.H. Jordan, Thermal barrier coatings for gas-turbine engine applications, Science 4 (2002) 280–284.
[39] N. Qin, X.Q. Liu, X.M. Chen, Thermal expansion and high-temperature phase transion of $Ba_{6-3x}Ln_{18}Ti_{18}O_{54}$ (Ln=La, Nd, and Sm) ceramics, Journal of the American Ceramic Society 90 (2007) 2912–2917.
[40] Z.G. Liu, J.H. Ouyang, Y. Zhou, X.L. Xia, Phase stability and thermal expansion property of ZrO_2–$NdO_{1.5}$–$AlO_{1.5}$ ceramics from 50 to 1550 °C, Materials and Design 30 (2009) 1845–1849.
[41] H. Lehmann, D. Pitzer, G. Pracht, R. Vassen, D. Stover, Thermal conductivity and thermal expansion coefficients of the lanthanum rare-earth-element zirconates system, Journal of the American Ceramic Society 86 (2003) 1338–1344.